Experimental and numerical study of sloshing and swirling behaviors in partially loaded membrane LNG tanks

M. Arai & T. Yoshida
Yokohama National University, Yokohama, Japan

H. Ando
Monohakobi Technology Institute, Tokyo, Japan

ABSTRACT: It is well known that partial loading in the membrane LNG tanks may lead to a violent sloshing phenomenon and it can cause structural damages to the tanks. In this study, in order to understand the basic characters of sloshing, we carried out model experiments and measured the liquid global forces, sloshing pressures and liquid motion in the model tanks. In the model experiments, a liquid rotating motion in the tank (swirling) was observed in some test cases. Swirling phenomenon has not been discussed in detail in membrane tanks, however, in some cases we observed that the liquid motion became very violent. We, therefore, studied membrane tanks with different tank-length-to-tank-breadth ratio and examined the conditions of the occurrence of swirling. We also examined the sloshing loads in irregular waves and investigated the relationship between sloshing loads and ship's motion response spectra. A practical formula that predicts the sloshing load was obtained. The results obtained from this study are considered to be useful for not only the designers but also for the operators of LNG carriers.

1 INTRODUCTION

Due to the growing demand for natural gas in the world, numbers and size of Liquefied Natural Gas (LNG) Carriers are increasing. Also there appeared new topics related to the LNG cargo transportation such as the application of LNG carriers to the shuttle transportation of the produced natural gas from the Floating LNG (FLNG), adoption of LNG as the fuel for ships, etc. In these new transportation modes, partial filling in the LNG tank is inevitable. However, violent sloshing phenomena may occur in the partially loaded membrane LNG tanks, and it can cause structural damages to the tank. In this study, in order to understand the characters of sloshing, we carried out model experiments and measured the liquid global forces, sloshing pressures and liquid motion in the model tanks. In the model experiments, a liquid rotating motion in the tank, i. e., swirling, was observed in some test cases. Swirling phenomenon has been studied by some researchers but those researches were basically for rectangular tanks. For example, Faltinsen et al. 2005 utilized multi-modal approach and analyzed three-dimensional liquid motion in a square-base tank. Vaziri et al. 2015 used a fully non-linear potential theory and studied sloshing in four rectangular tanks with different length-to-breadth ratio. In Chen et al. 2010, a time dependent Finite Difference Method was used to simulate liquid sloshing in a rectangular tank. However, swirling phenomenon has not been discussed in detail for the prismatic tanks which have the shape of membrane tanks of LNG carriers. Also above mentioned studies were carried out with regular excitation. We, therefore, studied membrane tanks with different tank-length-to-tank-breadth ratio and examined the conditions of the occurrence of swirling. We also studied the sloshing loads in irregular waves and investigated the relationship between sloshing loads and ship's motion response spectra. A practical formula that estimates the sloshing load was obtained, and we applied it to predict the sloshing load in the tanks of an LNG carrier which navigates in the North Pacific Ocean. The results obtained from this study are considered to be useful for not only to the designers but also for the operators of LNG carriers.

2 MODEL EXPERIMENTS

2.1 *Experimental setup*

A series of model experiments were carried out at Monohakobi Technology Institute (MTI) Yokohama Laboratory, as shown in Figure 1. A 1:40 scale tank mounted on a moving table was used (Figure 1, left, Tank-L). The Tank-L is a scale model of a membrane tank with length x breadth x depth dimensions of 971 x 952 x 689 mm. Ten Kyowa PS-05KD pressure gauges were placed along the walls (see Figure 2). The moving table was excited with regular and

irregular sway motions. A smaller model tank of 1:68.75 scale was also used to measure the transverse and longitudinal forces acting on the tank (Figure 1, right, Tank-S) by using a two-directional load cell (see Figure 3). The internal shapes of the two tanks were exactly the same, and only the tank size was different.

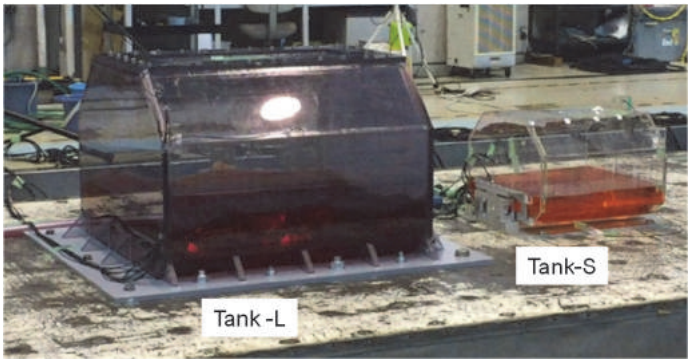

Figure 1. Model tank mounted on a moving table.

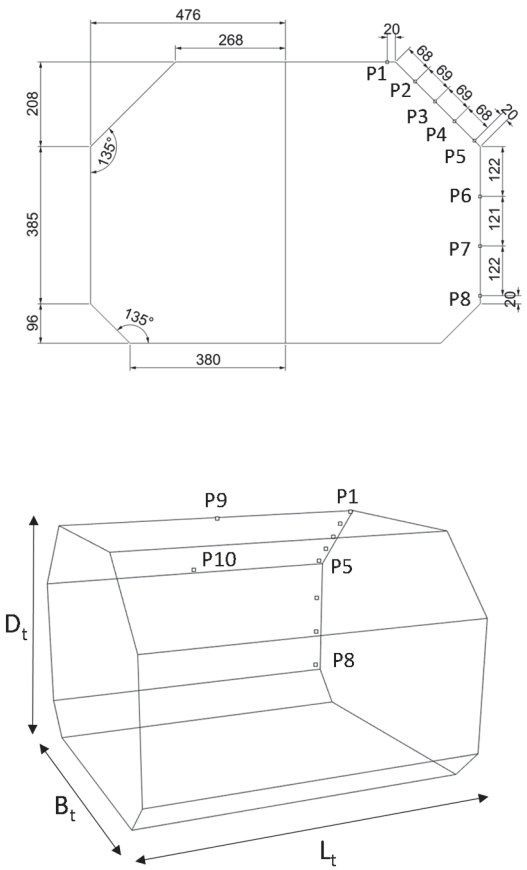

Figure 2. Model tank dimensions and pressure gauge locations (Tank-L, units in mm).

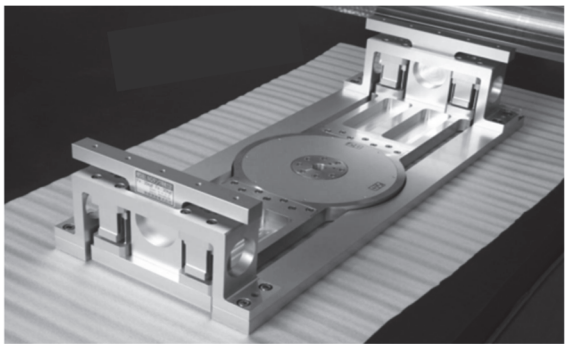

Figure 3. Load cell.

2.2 *Regular excitation experiments*

Sway excitation was applied to the large tank in the tank's lateral direction at its sloshing natural frequency while changing the filling level to 30, 50, 70, 80 and 90%.

Simple linear theory may be used for estimating the sloshing natural frequency of a tank having a rectangular cross sectional shape. The natural frequency of the tank when assuming a rectangular cross section is given by the following equation:

$$f_n = \frac{1}{2\pi}\sqrt{\frac{g\pi}{b}\tanh\frac{\pi h}{b}} \qquad (1)$$

where, h is the liquid height in the tank, b is the tank width, and g is the gravitational acceleration.

The actual membrane LNG tank has an octagonal cross section with chamfers where the tank width is narrow at top and bottom parts of the tank. Therefore, when the static liquid surface is in the vicinity of the tank ceiling and the tank bottom, the width of the free surface which is narrowed by the chamfers (i.e., $b=B'$) is used as the value of b in the equation (1) (see Figure 4).

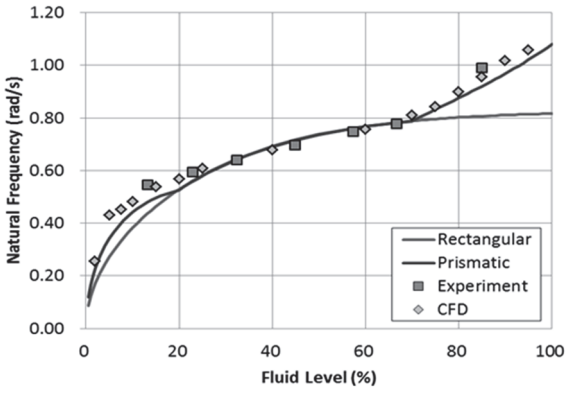

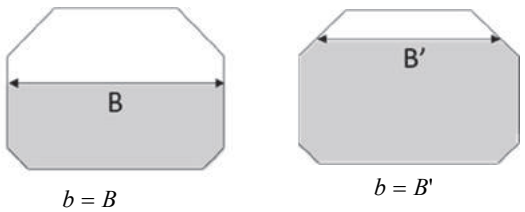

Figure 4. Estimation of 1st mode natural frequency.

As shown in Figure 4, the predicted natural frequencies of the chamfered tank by equation (1) agree well with the experimental and numerical values obtained from the preliminary studies carried out by Yokohama National University.

2.3 *Irregular excitation experiments*

Several ISSC-type wave spectra were prepared for the irregular excitation tests. Then the irregular excitation time series were created using the sway motion response amplitude operator (RAO) of an LNG carrier. Table 1 shows the tested irregular excitation conditions, where H_s is the significant wave height and T_{mean} is the mean wave period.

Table 1. Irregular test conditions.

Case	Filling level[%]	H_s [m]	T_{mean} [s]	Duration [s]
1	50	0.072 (4.95)	1.510 (12.52)	1200 (9950)
2	50	0.144 (9.9)	1.510 (12.52)	1200 (9950)
3	50	0.08572 (5.89)	1.152 (9.55)	1200 (9950)
4	50	0.144 (9.9)	1.124 (9.32)	1200 (9950)

Note: Values in parentheses indicate actual scale ones.

3 NUMERICAL METHOD

The numerical method used in the analysis of sloshing was based on the finite difference technique developed by the authors (Arai et al. 2002, 2006a, 2006b) for partial load conditions. The numerical method is outlined below.

The flow field in the tank is assumed to be three-dimensional, and the liquid is assumed to be incompressible and inviscid. The governing equations in the Cartesian coordinate system (x, y, z) fixed to the tank are the mass continuity equation:

$$\frac{\partial u}{\partial x}+\frac{\partial v}{\partial y}+\frac{\partial w}{\partial z}=0 \tag{2}$$

and Euler's equations of motion:

$$\frac{\partial u}{\partial t}+u\frac{\partial u}{\partial x}+v\frac{\partial u}{\partial y}+w\frac{\partial u}{\partial z}=-\frac{1}{\rho}\cdot\frac{\partial p}{\partial x}+f_x \tag{3}$$

$$\frac{\partial v}{\partial t}+u\frac{\partial v}{\partial x}+v\frac{\partial v}{\partial y}+w\frac{\partial v}{\partial z}=-\frac{1}{\rho}\cdot\frac{\partial p}{\partial y}+f_y \tag{4}$$

$$\frac{\partial w}{\partial t}+u\frac{\partial w}{\partial x}+v\frac{\partial w}{\partial y}+w\frac{\partial w}{\partial z}=-\frac{1}{\rho}\cdot\frac{\partial p}{\partial z}+f_z \tag{5}$$

in which the variables are defined as follows:
u, v, w: components of the velocity in x, y and z directions, respectively,
ρ : liquid density,
p: pressure,
f_x, f_y, f_z: external forces in x, y and z directions, respectively.

Change of the free surface of the liquid over time was calculated by the following equation:

$$\frac{\partial H}{\partial t}+u\frac{\partial H}{\partial x}+v\frac{\partial H}{\partial y}=w \tag{6}$$

where $H=H(t,x,y)$ is the vertical position of the free surface. This simplified expression of the free surface cannot treat the extremely local deformation of the free surface such as spray. However, the present method has the excellent feature of numerically stable computation and can also simulate the violent flow in the tank, including the impact of the liquid on the tank ceiling.

4 COMPARISON AND DISCUSSION OF MODEL TEST AND NUMERICAL RESULTS

4.1 *Sloshing pressure*

Figure 5 compares the measured and computed pressure time histories of 50% filling case. Regular excitation was given and the pressure at P5 (lower part of the chamfer (see Figure 2) and at P8 (lower part of the side wall) were shown.

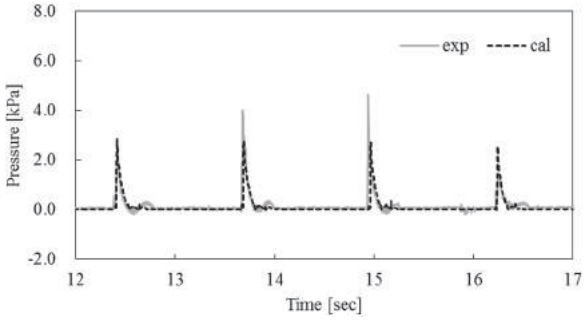

(a) P5

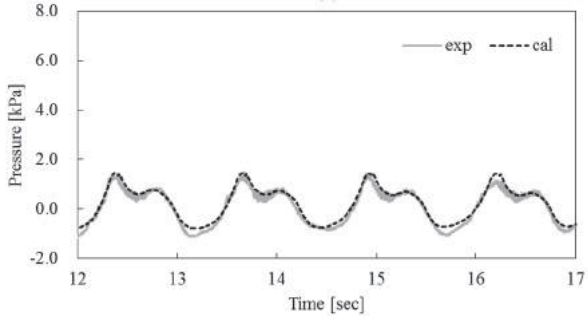

(b) P8

Figure 5. Pressure histories.

4.2 *Hydrodynamic force on tank wall and effect of tank size*

Figure 6 shows an example of the computed force time histories. In Figure 6, the magnitude of the force is non-dimensionally expressed using: liquid density (ρ), gravitational acceleration (g), tank length (L_t), tank breadth (B_t) and liquid height (h). Regular sway motion was applied to the tank. F_y is the computed lateral force component, and F_x is the longitudinal force component. As an initial condition of the numerical simulation, the free surface was given a small inclination (i.e., 1 degree) to generate the swirling motion. This small initial disturbance was necessary since, without the disturbance, it was difficult to generate the swirling motion in the numerical simulation. At the beginning of the simulation, only F_y was generated as shown in Figure 6, but after a period of time, swirling motion started, and the amplitude of F_x increased to be almost the same as that of F_y. From this figure, it can be said that the ratio F_x/F_y can be used as an index with which to judge the occurrence of swirling.

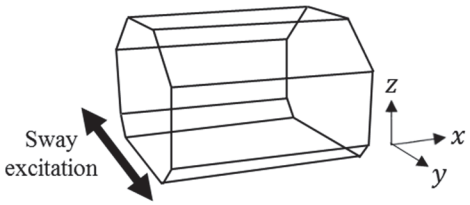

(a) Direction of excitation

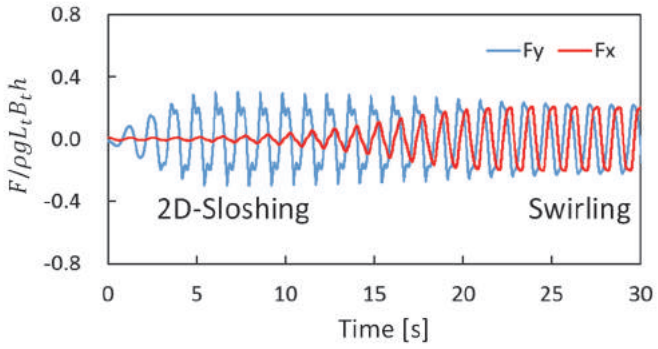

(b) Force histories

Figure 6. Direction of excitation and force histories.

As presented in Figure 6, the occurrence of swirling was easily distinguished by the emergence of the longitudinal force (F_x). In this study, the tank breadth (B_t=952 mm) was kept constant and the tank length was changed for several cases, and the computed results were examined. The tanks were excited with a regular sway excitation with a 20-mm amplitude at the natural sloshing period. Figure 7 summarizes the computed F_x/F_y ratio for tanks with different L_t/B_t ratios for two conditions, 30% and 50% filling levels, respectively. It can be clearly seen that the swirling occurred with high intensity when the L_t/B_t ratio was near 1.0. For both cases, swirling occurred in the range $0.9 < L_t/B_t < 1.10$. As for the filling level, we observed that swirling occurred when the filling level was between 30% and 70%.

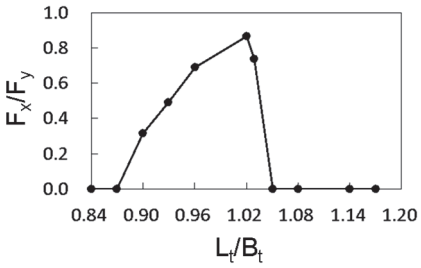

30% filling level

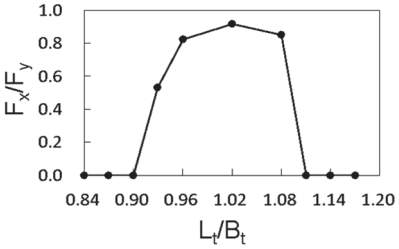

50% filling level

Figure 7. Computed F_x/F_y for different L_t/B_t ratios.

4.3 *Comparison between experimental results and numerical results of irregular excitation experiments*

In order to study the sloshing response in irregular seaways, we excited the model tank (Tank-S) on a moving table with irregular sway motions. The time histories of the tank's sway motion were prepared using the typical wave spectrum data as shown in Table 1 and the ship's sway motion RAO (Response Amplitude Operator). Examples of the measured and computed time histories of F_x and F_y are shown in Figure 8. The force and time scales in Figure 8 are converted from the model scale to the actual ship scale using Froude's law.

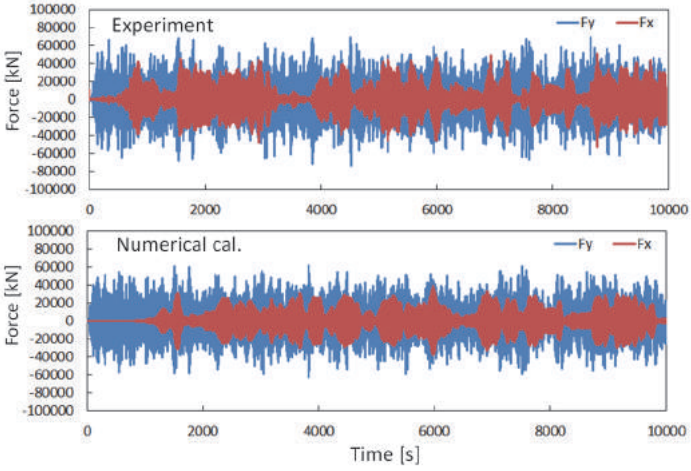

Figure 8. Comparison of measured and computed force histories (50% filling, irregular sway motion, $H_{1/3}$=5.89 m, T_{mean}=9.55 s on actual ship scale).

Although, the same time history of the tank motion was used in the model experiment and the numerical simulation, the measured and computed force histories did not perfectly match each other. One possible reason for this is the difference in the rotating direction, i.e., clockwise or anti-clockwise, of the liquid motion in the tank. As observed in the model experiments with regular excitation, a small disturbance in the flow can trigger the swirling and determine the direction of the rotating motion. Incidentally, either clockwise or anti-clockwise motion may start. The swirling motion couples with the sloshing motion, and the accumulated liquid motion response changes the liquid motion time history afterward. Therefore, it was very difficult to numerically simulate the time histories of the force under irregular excitation. However, in some parts of the force time histories, very similar patterns were reproduced by our numerical computation. One example of such a case is shown in Figure 9 and Figure 10. A part of the time histories presented in Figure 8 is shown with an enlarged time scale in Figure 9 (F_y) and Figure 10 (F_x). As shown in Figure 9, the computed F_y, the lateral force, agrees well with the measured one in this time period (Figure 9(a)). On the other hand, the computed F_x, the longitudinal force, did not match the measured one (Figure 10(b)). As shown in Figure 10(c), however, if we reverse the sign of the force it agrees quite well with the measured data. This means that the rotating direction of the numerical simulation (Figure 10(b)) was opposite that of the measured one.

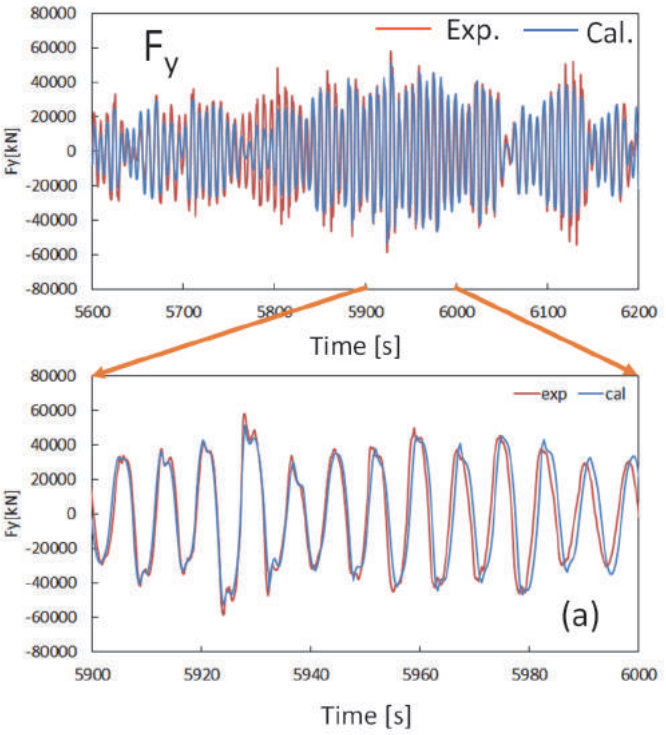

Figure 9. Comparison of measured and computed force histories of F_y (part of Figure 8 is enlarged in time, irregular sway motion, $H_{1/3}$=5.89 m, T_{mean}=9.55 s on actual ship scale).

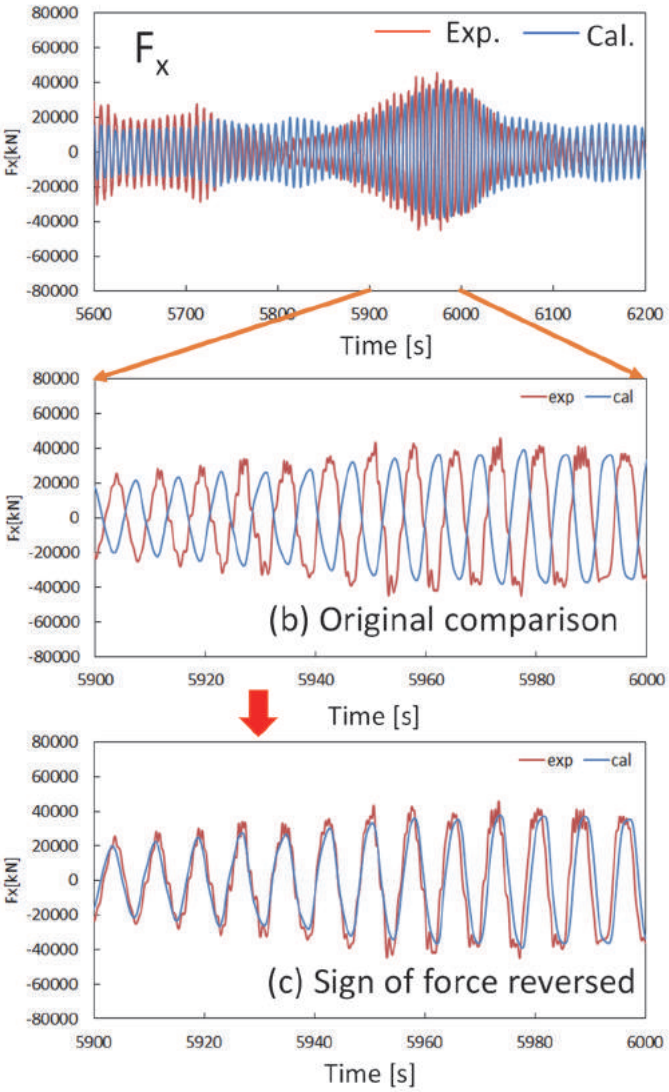

Figure 10. Comparison of measured and computed force histories of F_x (part of Figure 8 is enlarged in time, irregular sway motion, $H_{1/3}$=5.89 m, T_{mean}=9.55 s on actual ship scale).

4.4 *Effect of L_t/B_t and size of actual tanks*

Sloshing responses in irregular excitation for the tank with different L_t/B_t were studied. The same irregular excitation used for the case shown in Figure 8 was applied. Figure 11 presents the results and again it can be seen that the swirling occurred with high intensity when the L_t/B_t ratio was near 1.0. For these cases, swirling occurred in the range $0.9 < L_t/B_t < 1.10$.

In order to examine the L_t/B_t ratio of the actual LNG tanks, we collected the tank size information of 14 constructed or designed membrane-type LNG carriers, and 6 of them had tanks that met the above-mentioned criterion (i.e., $0.9 < L_t/B_t < 1.10$). Table 2 presents the tank dimensions of those ships. If the liquid cargo is partially loaded in the tanks with the tank length to tank breadth ratio near 1.0, swirling is expected to occur.

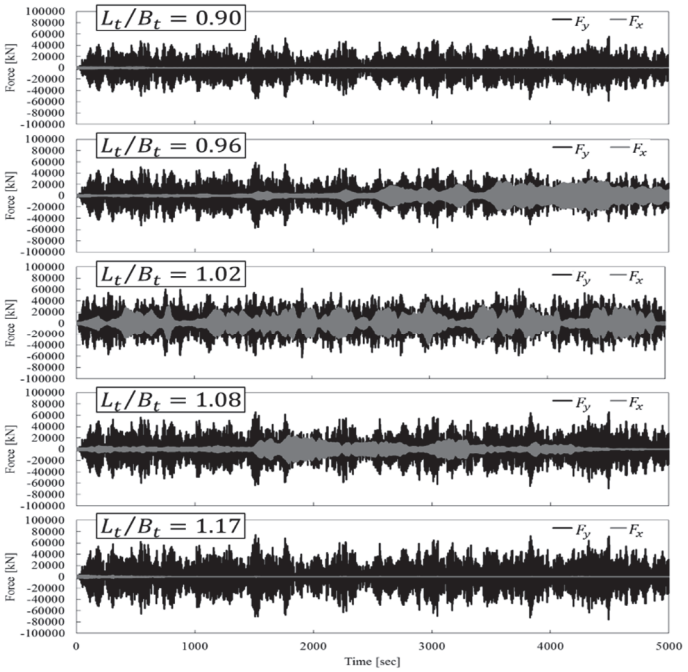

Figure 11. Force histories by irregular excitation for different L_t / B_t ratios.

Table 2. Tank L_t / B_t ratios of actual or designed ships.

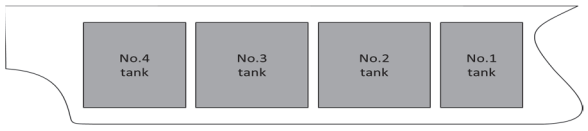

Ship	NO.4 Tank			No.3 Tank			No.2 Tank			No.1 Tank		
	L_t(m)	B_t(m)	L_t/B_t	L_t(m)	B_t(m)	L_t/B_t	L_t(m)	B_t(m)	L_t/B_t	L_t(m)	B_t(m)	L_t/B_t
1	46.05	42.65	1.080	46.05	42.65	*1.080	46.05	42.65	*1.080	31.09	36.53	0.851
2	46.05	40.31	1.142	46.05	40.31	1.142	46.05	40.31	1.142	35.50	36.80	*0.965
3	49.60	49.90	*0.994	49.60	49.90	*0.994	49.60	49.90	*0.994	39.87	40.57	*0.983
4	47.07	41.63	1.131	47.07	41.63	1.131	47.07	41.63	1.131	33.81	32.11	*1.053
5	38.28	37.81	*1.012	43.58	37.81	1.153	43.89	37.81	1.161	Wedge Shape		
6	40.00	37.81	*1.058	44.75	37.81	1.184	44.75	37.81	1.183	31.45	33.75	*0.932

*indicates the tank with $0.90 < L_t/B_t < 1.1$

5 SLOSHING LOAD ESTIMATION IN ACTUAL SEAS

As shown in Section 4.3, measured F_y histories in irregular waves can be reasonably reproduced by the numerical method. Figure 12 presents the return period of the peak value of F_y where zero-up cross method was applied to obtain the peak value of F_y. In Figure 12, numerical values by two dimensional (2D) and three dimensional (3D) computations are compared with experimental ones. In this study, 2D computation means that the mesh division in the longitudinal direction of the tank is not considered and 2D flow in the tank's transverse section is solved. Therefore, swirling phenomenon is not reproduced by the 2D computation. Figure 12 shows a certain value of peak F_y emerges once in a certain "return period". By fitting the distribution function of the Weibull distribution to the measured and computed values, we estimated the maximum peak value of F_y in three hours. Since there is a tendency that the F_y in the swirling phase is a little smaller than that in the sloshing phase, the results of 2D computation becomes slightly larger than the measured and 3D computation values. However, the differences between them are not significant, and we can conclude that the measured responses of F_y by irregular excitation can be reproduced by both 2D and 3D computations.

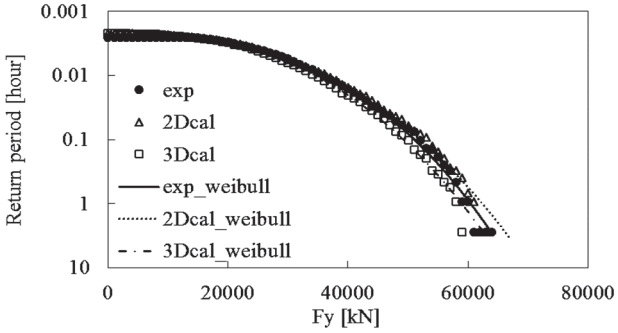

Figure 12. Return period (50% filling, $H_{1/3}$=5.89 m, T_{mean}=9.55 s on actual ship scale).

In order to obtain the relationship between the tank excitation and the generated sloshing load, the numbers of the peak values in the time histories of F_y was counted by zero-up cross method. Results of the counted peak numbers are shown in Table 3.

Table 3. Number of sloshing.

Case	Number of peak observed	Number of excitation	(Duration of exp.) / T_N	3 hour maximum [kN]
1	1539	1047	1284	39209
2	1492	684		52376
3	1394	906		64099
4	1365	1099		81096

As shown in Table 3, the number of peaks obtained by the F_y histories do not agree with the number of excitations (i.e., the number of encounter waves). On the other hand, they are close to the number of peaks estimated by the natural period of sloshing motion of the tank (T_N). It seems that the liquid sloshing numbers in the tank by the irregular tank excitation is not determined by the tank excitation but is determined by the natural period of sloshing. This may lead to the possibility that the component of the irregular excitation which has the sloshing natural period dominates the phenomenon. Then let us focus on the magnitude of the tank sway motion spectrum at the sloshing natural frequency (see $\Phi(f_N)$ of Figure 13).

Figure 14 indicates the relation between the maximum F_y values in three hours and the $\sqrt{\Phi(f_N)}$. Fig-

ure 14 suggests that there is a strong relation between $\sqrt{\Phi(f_N)}$ and F_y. By applying the least squares method to the data shown in Figure 14, we obtained a formula that can be used to estimate the global sloshing load to the tank's side wall as:

$$F_y = 3.3\times10^4\sqrt{\Phi(f_N)} + 1.4\times10^4 \quad (7)$$

Note that the equation (7) is adjusted to be used for the actual scale LNG tank considering the density of the liquefied natural gas.

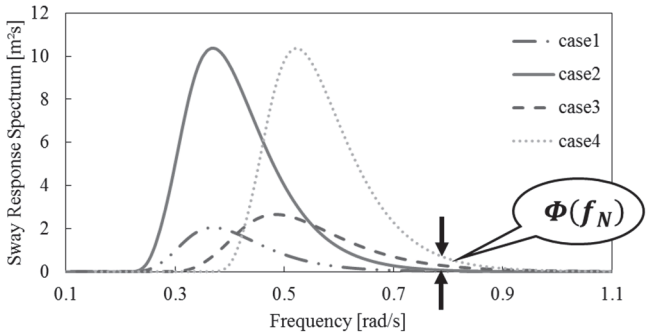

Figure 13. Sway response spectra of small tank (full scale).

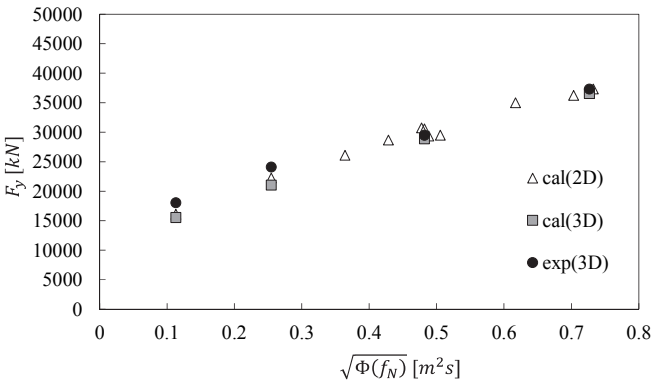

Figure 14. Correlation between F_y and $\sqrt{\Phi(f_N)}$.

Figure 15 shows the flow to estimate the sloshing load in a certain sea area. As an example of sloshing load estimation based on the flow presented in Figure 15, 3-hour maximum value of the global sloshing load exerted on the tank side wall was obtained for each of the sea area in the North Pacific Ocean in winter (see Figure 16). Although we need to further advance the method to include all of the six ship motion components other than only sway motion, we can grasp the general tendency of the level of sloshing severity in the ocean by Figure 16. For example, the area between Japan and the US in the north part of the Pacific Ocean is the harsh area from a sloshing point of view.

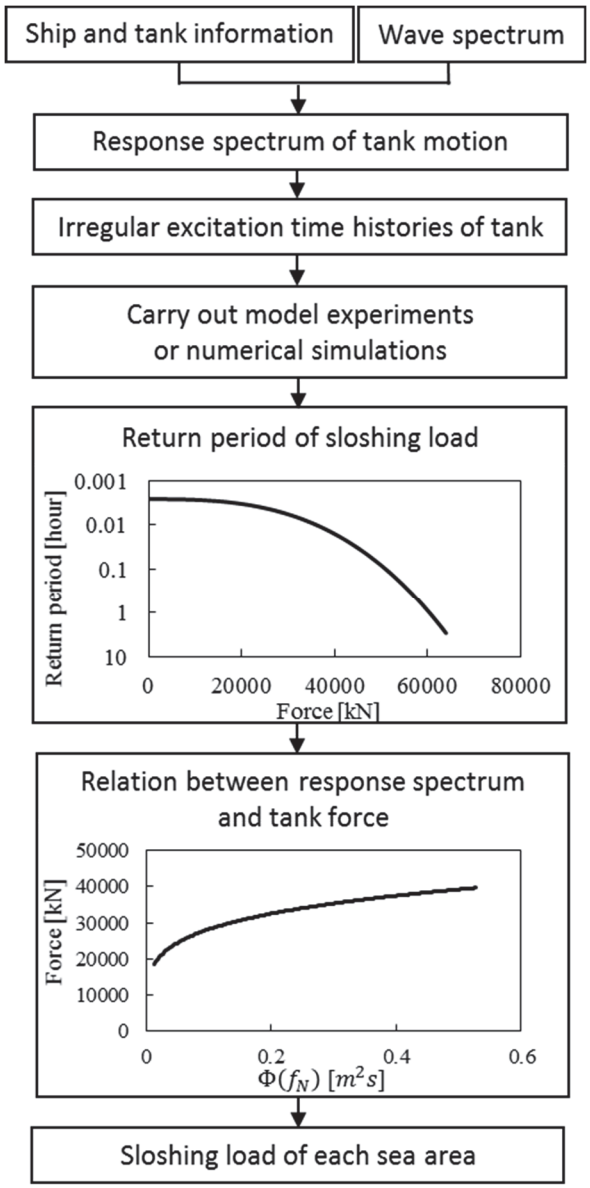

Figure 15. Flowchart of estimating sloshing load.

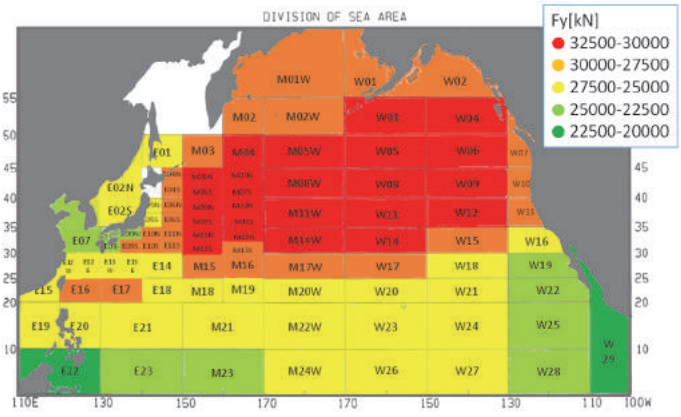

Figure 16. Distribution of F_y in the North Pacific Ocean in winter.

6 CONCLUSIONS

In this study, the basic characters of sloshing in membrane LNG tanks were studied. From this study, we obtained the following results:

- Swirling occurs if the membrane tanks have the tank length to tank breadth ratio between 0.9-1.1 and filling level between 30%-70%. There exist a considerable number of LNG carriers which have such tank length to tank breadth ratio.

- Although swirling load is in general smaller than the sloshing one, it should be noted that the load distribution pattern of swirling differs from that of sloshing.

- Global tank load can be evaluated reasonably by our numerical method.

- We proposed a flow to estimate the sloshing load using the wave spectrum and the RAO of the ship.

- By using the proposed method, global sloshing load exerted on the tank side wall was obtained for each of the sea area in the North Pacific Ocean in winter.

PREFERENCES

Arai, M., Cheng, L.Y., Kumano, A., Miyamoto, T. 2002. A technique for stable numerical computation of hydrodynamic impact pressure in sloshing simulation, *Journal of Society of Naval Architects of Japan*, Vol.191, 299-307.

Arai, M., Makiyama, H.S., Cheng, L.Y., Kumano, A., Ando, T. 2006. Numerical and experimental study of 3-D sloshing in tanks of LNG carriers, *Proceedings of OMAE 2006*, Paper No. OMAE 2006-92235.

Arai, M., Makiyama, H.S., Cheng, L.Y., Kumano, A., Ando, T., Imakita, A. 2006. Numerical analysis of 3-D sloshing in tanks of membrane-type LNG carriers, *ICSOT, Design, Construction & Operation of Natural Gas Carriers & Offshore Systems*, 201-209.

Chen B. F., Wu C. H. 2010. Effects of excitation angle and coupled heave-surge-sway motion on fluid sloshing in a three-dimensional tank, *Journal of Marine Science and Technology*, Vol. 16, 22-50.

Faltinsen O. M., Rognebakke O.F., Timokha, A. N. 2005. Classification of three-dimensional nonlinear sloshing in a square-base tank with finite depth, *Journal of Fluids and Structures*, Vol. 20, 81-103.

Karuka, G.M., Arai, M., Ando, H. 2017. Sloshing and swirling in partially loaded prismatic chamfered tanks, *Proceedings of OMAE 2017*, Paper No. OMAE 2017-61562.

Vaziri N., Chern M. J., Borthwick A. G. L. 2015. Effects of base aspect ratio on transient resonant fluid sloshing in a rectangular tank: a numerical study, *Ocean Engineering*, Vol. 105, 112-124.